

## Lidar observation of a strongly nonlinear internal wave train in the Gulf of Alaska

J. H. CHURNSIDE<sup>†</sup> and L. A. OSTROVSKY<sup>‡</sup>

<sup>†</sup>NOAA Environmental Technology Laboratory, 325 Broadway, Boulder, Colorado 80305, USA; Email: james.h.churnside@noaa.gov

<sup>‡</sup>Zel Technologies/NOAA Environmental Technology Laboratory, 325 Broadway, Boulder, Colorado 80305, USA; Email: lev.a.ostrovsky@noaa.gov

(Received 10 April 2003; in final form 25 March 2004)

This paper demonstrates the observation of what appears to be a partially developed solitary internal wave group using an airborne lidar over the Gulf of Alaska. The probable generation mechanism is the interaction of the tide with the continental shelf 130 km away. Detection by lidar was possible because of a planktonic layer associated with a shallow pycnocline.

### 1. Introduction

Observations of solitary internal waves, or internal solitons, span several decades. Most of the data refer to coastal zones where trains of pulse-like pycnocline displacements close to solitary waves ('solibores') are regularly observed in many areas. They are attributed to transformation of energy from barotropic tides into internal waves through an interaction with the shelf break or other bottom features (banks, sea mounts, etc.). Solitons are also observed in the open ocean, at least near the shelf, in deep water as far as 300–500 km from shore. Reviews of internal soliton observations can be found in Ostrovsky and Stepanyants (1989) and Duda and Farmer (1999).

Remote observations of internal solitons are available mostly from satellite photographs and radar (especially Synthetic Aperture Radar (SAR)) images of soliton groups. For deep seas they are only rarely matched with *in situ* measurements. *In situ* observations of internal waves were supplemented by satellite sensor data in the Sulu Sea (Apel *et al.* 1985, Liu *et al.* 1985). These solitons were generated by the barotropic tide interacting with a bank, and were observed at distances up to 300 km from the coast, where the ocean depth was greater than 3000 m.

Origins of deep-sea solitons are not always clear. However, at least for the off-shelf areas with a shallow pycnocline, it is most probable that, similarly to the on-shelf solitons, they are generated by barotropic tides at shelf breaks and propagate into the open ocean (Konyaev and Sabinin 1992).

For a theoretical description of solitary waves of moderate amplitude in shallow water, the Korteweg–de Vries (KdV) equation and its numerous modifications are commonly used. For deep water, KdV and its generalizations are not applicable. The Benjamin–Ono (BO) equation corresponds to a thin upper layer and an infinitely deep lower layer (for references, see, e.g. Ostrovsky and Stepanyants 1989). Note that very strongly nonlinear solitons have been observed on the shelf (Pingree and Mardell 1985, Stanton and Ostrovsky 1998), and the corresponding theoretical

consideration has been done for them. In the observations of which we are aware, the pycnocline displacement of deep-sea solitons is moderate relative to its initial depth, and the waves are weakly nonlinear. Even in strong internal waves observed in the Sulu Sea (Liu *et al.* 1985), wave amplitudes reached only 70 m at an initial pycnocline depth of 200 m. Still, some theoretical models were recently suggested for strongly nonlinear waves in a thin upper layer over an infinitely deep lower fluid. Choi and Camassa (1999) suggested a system of equations for strongly nonlinear waves, and Ostrovsky and Grue (2003) suggested a simpler evolution equation, which is a generalization of the BO equation, and compared the results with an exact numerical calculation.

In this paper we present a unique observation of a solitary wave group with some interesting properties. It is unique because it was the first observation of this phenomenon by a laser carried by an aircraft, so that the record was taken remotely and directly from an underwater layer (plankton layer) rather than from the surface signatures formed by the action of internal currents on surface waves. It is interesting in that the nonlinearity of the wave is remarkably strong; it shows soliton-like depressions of the layer from about 3.5–4 m to about 9.5 m, together with the subsequent general depression to about 7.5 m, which is presumably due to the tidal motions. Also, the distance between solitons, about 60 m for the first few, is comparable with the width of each pulse; this indicates that the observed ‘solibore’ was in an evolving stage where the solitons are not strongly separated.

Detection of an internal wave group with an airborne lidar requires a scattering layer that is associated with the pycnocline, or at least with an isopycnal level. There is some evidence that this can happen. Hanson and Donaghay (1998) measured a thin layer of high chlorophyll concentration in East Sound, Orcas Island, Washington State. The top of this 1-m thick layer was at the maximum density gradient at a depth of just over 2 m. Cowles *et al.* (1998) presented the results of fluorometer measurements 100 miles off the Oregon coast. They demonstrate a layer of enhanced chlorophyll at the 24.966 isopycnal, which varied in depth from about 35 to 38 m. Warren *et al.* (in press) showed a strong correlation between the depth of the chlorophyll maximum and the depth of the 28.7 isopycnal in the Ligurian Sea north of Corsica.

If the pycnocline is close enough to the surface, these layers can be observed by an airborne lidar. Hoge *et al.* (1988) reported specifically on the detection of layers. More recently, Vasilkov *et al.* (2001) reported detection of similar layers using a polarization lidar. The lidar signal characteristics of a subsurface layer have also been modelled using a Monte Carlo approach (Krekov *et al.* 1998a,b).

We could find no report of the detection of internal waves perturbing these layers measured from an airborne lidar. Walker *et al.* (1982) detected an internal wave from a lidar mounted on a ship. They used the lidar signal at a depth of 19.2 m to infer the presence of an internal wave with peak to peak amplitude of about 2 m on a thermocline at this depth.

In what follows we shall describe the experimental data and evaluate parameters of the observed impulses from the viewpoint of soliton theory. We show that these parameters are consistent with what one would expect from tidally generated internal waves created at the edge of the continental shelf. We use the assumption that the scattering layer is associated with an isopycnal level, and that the measured cross-section represents a propagating wave and not just a static disturbance. The latter is not proven, but the use of towed sensors to measure internal waves from similar two-dimensional vertical sections is a well-established technique (Garrett and Munk 1979).

## 2. Materials and methods

The NOAA fish lidar is an airborne pulsed lidar (Churnside *et al.* 2001). A block diagram is presented in figure 1. The major components are: (1) the laser and beam-control optics; (2) the receiver optics and detector; and (3) the data-collection and display computer. The receiver telescope and the laser are mounted side by side, and the system was aimed downward through a hole in the bottom of a small twin-engine aircraft, flying at an altitude of 300 m. To reduce direct surface reflections, the lidar was directed at an angle of  $15^\circ$  from nadir.

The laser is a Neodymium-doped Yttrium Aluminium Garnet (Nd:YAG). It includes a fast optical switch (known as a Q-switch) which is opened after the laser crystal is fully charged, so that all of the energy is extracted in a short pulse. It also includes a nonlinear optical crystal to convert the laser light from infrared (1064 nm) to green (532 nm). This laser produces about 100 mJ of green light in a 12 ns pulse at a repetition rate of 30 Hz. The laser is polarized linearly and the beam is diverged, using a lens in front of the laser. The divergence is chosen so that the irradiance at the sea surface satisfies the US standard for exposure to laser light in the workplace (ANSI 1993). This irradiance level is also safe for marine mammals (Zorn *et al.* 2000). The diverged beam is directed by a pair of mirrors so that it is parallel to the axis of the telescope.

The receiver optics comprise a 17-cm diameter refracting telescope with a polarizing filter. The filter passes only that component of the reflected light for which the linear polarization is orthogonal to the polarization of the laser. The cross-polarized component was used because it produces the best contrast between fish and smaller scatterers in the water. This was determined during ship tests of the lidar, where the depolarization of the return from fish was about 30% and the depolarization of the water return was only about 10% (Churnside *et al.* 1997).

To reject background light, the light collected by the telescope passes through an interference filter. Background light is also reduced by an aperture at the focus of the primary lens that matches the field of view of the telescope with the divergence of

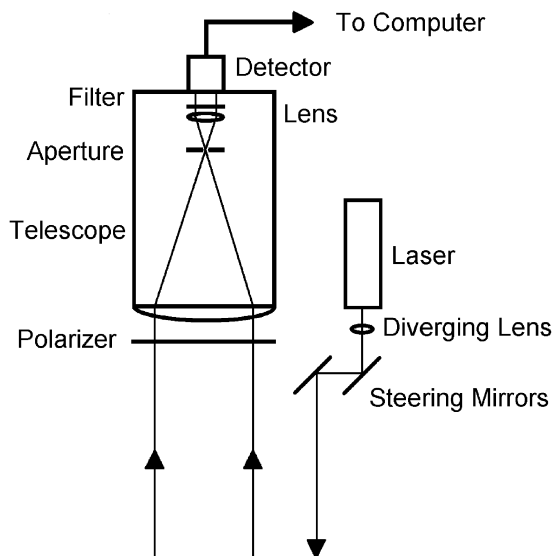


Figure 1. Schematic diagram of NOAA fish lidar.

the transmitted laser beam. The resulting light is incident on a photomultiplier tube (pmt), which converts the light signal into an electrical current. A  $50\ \Omega$  load resistor converts the current signal to a voltage, which is transformed with a logarithmic amplifier and digitized at 1 GHz with 8 bits of resolution (256 levels). This sample rate corresponds to a resolution of 0.11 m in depth. The amplifier has an input voltage range from  $-0.2\text{ mV}$  to  $-2\text{ V}$  which produces an output voltage range of about  $-0.024\text{ V}$  to  $-0.524\text{ V}$ , so that  $V_{\text{out}} = -0.125 \log(-V_{\text{in}}) - 0.486$ . Since the output voltage range is well within the range of an 8-bit digitizer, the logarithmic amplifier increases the maximum possible dynamic range from 256 to about  $10^4$ .

In addition to the log-transformed voltage signal, the computer records the aircraft position from the Global Positioning System (GPS), GPS time, the voltage applied to the pmt, and the attitude of the aircraft as measured by tilt sensors and laser gyroscopes on the optical package. The pmt voltage is used to calculate the gain of the tube, which is necessary for calibration. The computer also displays the data in real time during the flight.

The lidar was installed in a Beechcraft King Air 90. On 24 May 2002 (local time), it was flown from Kodiak to Juneau, Alaska, along the direct route at a speed of  $90\text{ m s}^{-1}$ . Figure 2 is a chart of the flight track. Figure 2(a) is a chart of the Northwest Pacific Ocean showing the flight track and the extent of the detailed chart. Figure 2(b) is a more detailed chart, which also shows the 200 m isobath, which is a good definition of the edge of the continental shelf in this region. The flight track extended from about  $152.2^\circ\text{ W}$  to  $135.3^\circ\text{ W}$  and crossed the edge of the shelf twice, at  $148.8^\circ\text{ W}$  and  $138.9^\circ\text{ W}$ .

### 3. Results

Figure 3(a) represents the primary result of this paper. The first part shows the relative lidar response as greyscale as a function of distance along the flight track and depth. We removed the effects of variations in aircraft altitude by locating the surface at the first peak of the lidar return in each pulse. We corrected the data for geometric loss, although the effect is small. We also corrected for the exponential attenuation of the signal using an attenuation coefficient of  $0.4\text{ m}^{-1}$ , which was measured from the lidar return in the upper layer. Several features are clear in this figure. The first is the presence of a clear scattering layer in the upper ocean. The second is a strong vertical oscillation of this scattering layer with the characteristics of an internal-wave soliton train. Finally, we note that the layer is deeper on one side of the wave group than on the other. These features are even clearer in figure 3(b), which is a plot of the depth of the maximum return from each lidar pulse across the internal wave train.

The position of this wave group is marked on the chart in figure 2. The position is  $142.874^\circ\text{ W}$  longitude,  $58.2402^\circ\text{ N}$  latitude. The time was 2:57 UTC on 25 May. It is about 130 km from the continental shelf in water that is about 4000 m deep.

This area of the ocean was not being observed by Synthetic Aperture Radar (SAR) at the time of the lidar observation, but a similar internal wave group was observed to the south-west. Figure 4 is the ScanSAR wide B quicklook image taken at 2:58:08 UTC on 25 May and processed at the Alaska Satellite Facility. It clearly shows a strong internal wave group with a leading edge at about  $135.68^\circ\text{ W}$  longitude,  $54.96^\circ\text{ N}$  latitude. This point is about 200 km from the continental shelf in water that is about 2700 m deep. The wavelength of this wave is about 4600 m, much longer than the one

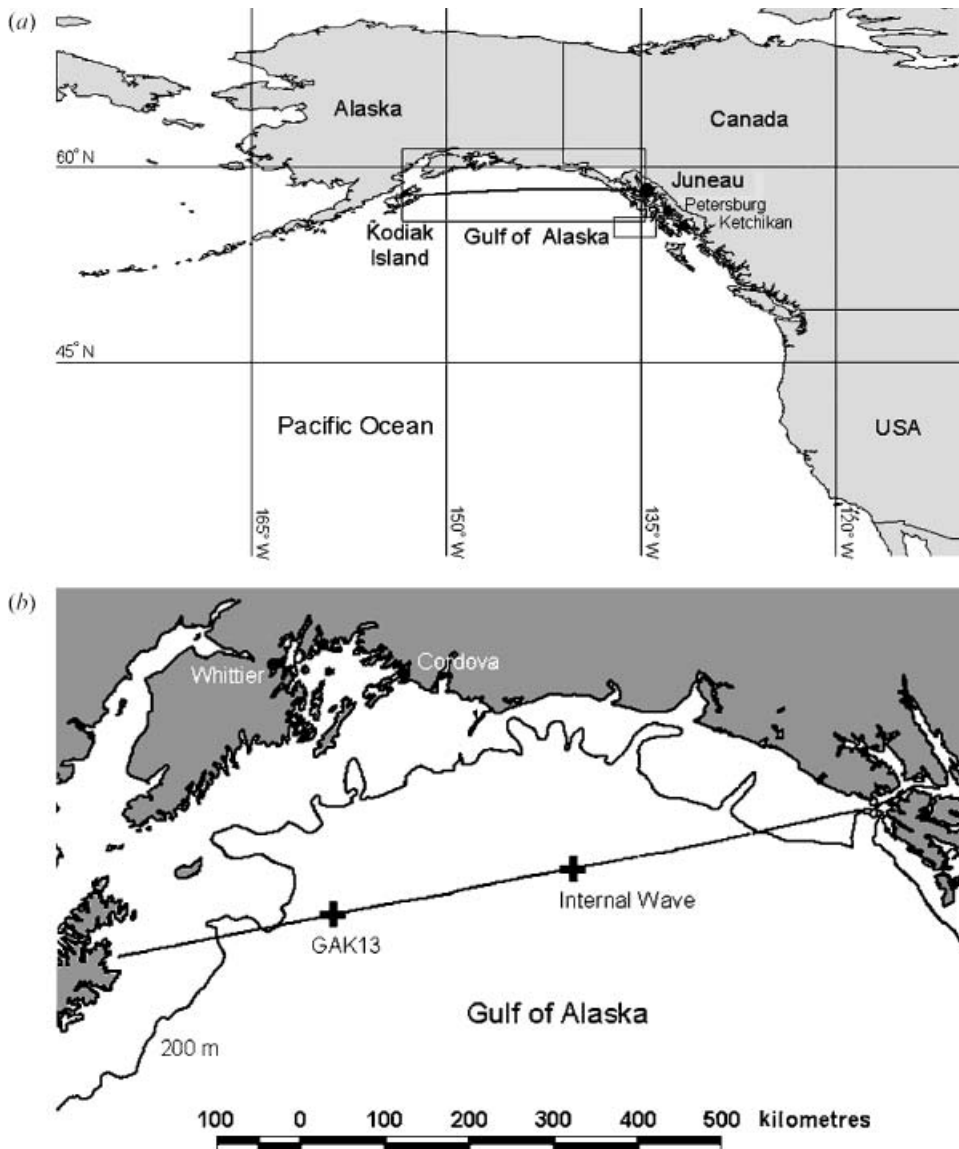


Figure 2. Chart with flight track from Kodiak to Juneau, Alaska. (a) Overview of the Northwest Pacific, with the location of the detailed chart denoted by the large rectangular box just above the 'Gulf of Alaska' label. A smaller rectangular box, overlapping the lower right-hand corner of the first, shows the region of figure 4. (b) A more detailed chart, including the 200 m isobath to represent the approximate edge of the continental shelf. The positions of the internal wave and the GAK13 oceanographic station are also marked.

observed in the lidar. In fact, the radar resolution in this mode of operation is about 200 m, so the wave group of figure 3 would not have been seen in this type of image.

#### 4. Discussion

At the time of year of this observation, the Gulf of Alaska supports large concentrations of plankton that are highly variable. This is shown in figure 5, which

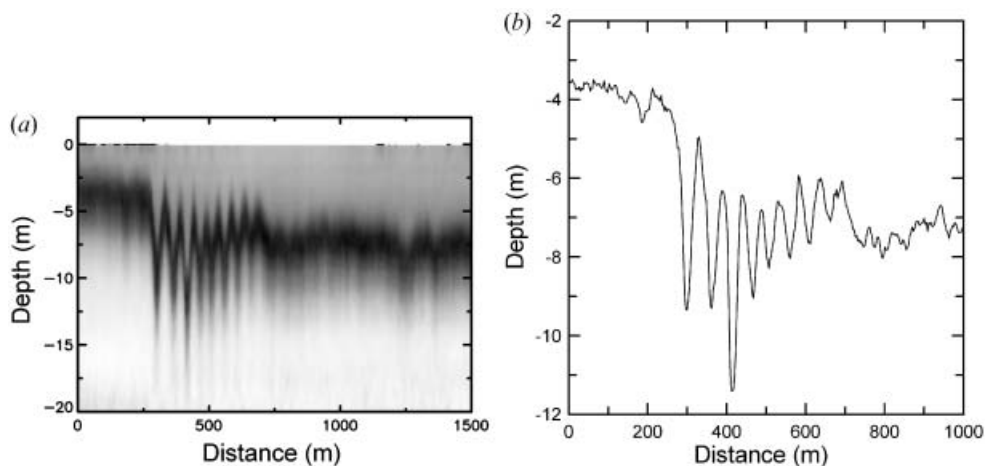


Figure 3. Lidar observation. (a) Lidar return as function of depth and distance along flight track, with darker grey representing more return energy. (b) Depth of maximum lidar return as a function of distance along the flight track.

is the Sea-viewing Wide Field-of-view Sensor (SeaWiFS) image of chlorophyll concentration averaged over the week ending on the day of the flight. The flight track and the position of the internal wave are marked on the figure. Note that the internal wave is located in a region where the colour image shows a high chlorophyll concentration.

Another view of the general conditions of the plankton layer in the Gulf is provided by the depth of the layer measured along the flight track by the lidar. These data are presented in figure 6. The position of the internal wave is also marked in this figure. We see that it is in a region in the Gulf where the plankton layer is closer than average to the surface.

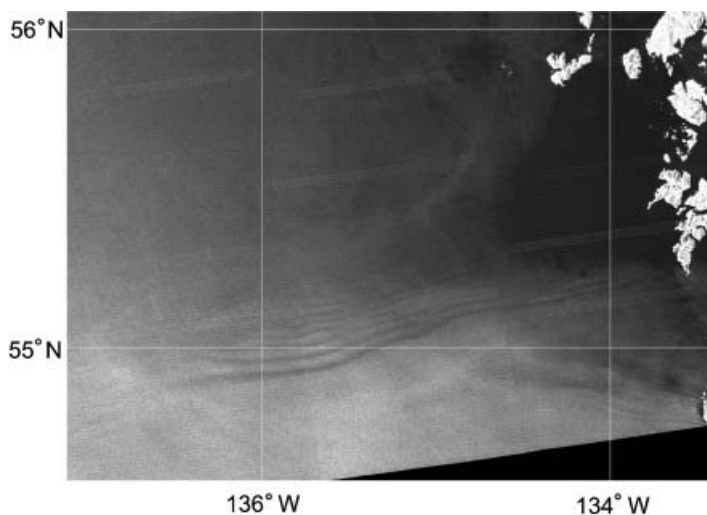


Figure 4. SAR image of internal waves in the Gulf of Alaska taken at about the same time as the lidar observation (2:58:08 UTC on 25 May) but a different location (copyright Canadian Space Agency 2002).

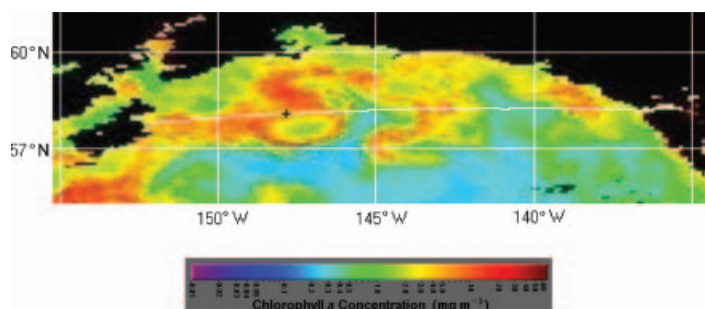


Figure 5. SeaWiFS image of chlorophyll concentration in the Gulf of Alaska. The curved white line is the flight track with the location of the observation marked by a white+ and the GAK13 location by a black+.

To compare the measured internal wave shape with theory, we need to know the density profile of the water. Unfortunately, few measurements exist for this area. The closest measurements of which we are aware were made at the Gulf of Alaska Station 13 (GAK13). This station lies right on the flight track (see figure 2), but the closest measurements were made at 19:15 UTC on 2 May, over three weeks before the flight. The temperature and salinity for depths between 2.5 and 20 m measured at that time were well mixed and apparently unable to support internal wave propagation within this layer. This seems consistent with figure 6, which shows a deeper scattering layer at that position. At the position of the internal wave train, however, the scattering layer is only about 4–5 m deep. A possible cause of this variability is a layer of fresh, less dense water over saltier seawater, which creates a pycnocline with a variable depth. The coast of south-east Alaska receives large amounts of precipitation (5.0 m annually in Whittier, 3.8 m in Ketchikan, 2.8 m in Petersburg, 2.4 m in Cordova). Figure 5 suggests a very complicated eddy structure in the Gulf of Alaska, which could advect patches of fresh water far offshore.

To make a rough estimate, we assume that the observed internal wave train was generated at the Alaska shelf break through transformation of a part of the energy of the barotropic, or surface, tide into an internal-wave mode. Such processes are known to be common for many areas of the ocean (e.g. Ostrovsky and Stepanyants

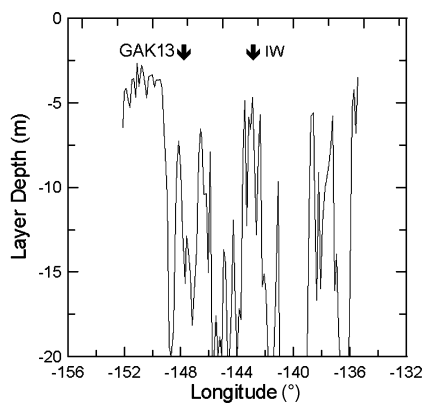


Figure 6. Depth of the scattering layer vs longitude along the flight track. The longitudes of the internal wave (IW) and the GAK13 station are marked.

1989, Grimshaw 2002). The Gulf has a rather large tidal range (about 4 m at Cordova at the time of this observation), and it would not be surprising to find this process at work here. According to a typical scenario, the nonlinear internal wave front steepens in the course of propagation, resulting in the appearance of oscillations and then the formation of a solibore consisting of pulse-like pycnocline displacements, each close to solitary waves; a number of such processes are described in Duda and Farmer (1999). In most cases, however, wave groups propagating toward the coast were observed, whereas in our case the wave propagated offshore and was observed in the deep sea. When a wave is propagating toward the shore, the water and, generally, the pycnocline are both getting shallower and contribute to the steepening wave (Zheng *et al.* 2001). For propagation away from shore, the bottom is not a factor, and the pycnocline must get shallow enough to cause the wave to steepen.

Let us make a few theoretical estimates. Weakly nonlinear theories like KdV predict the spacing and amplitude of the impulses to change with position in the train because of the linear dependence of soliton velocity on amplitude. Our observation suggests that the amplitudes and spacings are much more uniform than that, at least for the first few impulses. Therefore, we will use a strongly nonlinear theory proposed by Ostrovsky and Grue (2003). For a stronger nonlinear wave, the velocity depends less on amplitude. As a result, the disintegration into a soliton train occurs more slowly, and the energy transfer from rear solitons to forward solitons is weaker. Under these conditions, the differences in amplitude, spacing, and width are less than predicted by weakly nonlinear theories. Besides, the initial form of the tide-generated internal wave is far from the step function from which the greatest frontal soliton would develop. Observations by Stanton and Ostrovsky (1998) and Trevorrow (1998) support these predictions for the impulses at the beginning of the observed train.

First, we assume that the initial duration of the internal wave near the shelf is about 6 h (elevation phase of the semi-diurnal tide), and a relatively sharp pycnocline exists at a depth  $h \ll H$ , where  $H$  is the total depth of the sea. We can write a local wave velocity,  $c(z)$  at a point with the displacement (depression)  $z$  of the pycnocline, as (Ostrovsky and Grue 2003)

$$c(z) = c_0 \left( 3\sqrt{1 + z/h} - 2 \right) \quad (1)$$

where  $c_0 = \sqrt{g'h}$ ,  $g' = g\Delta\rho/\rho$ ,  $\rho$  is water density, and  $\Delta\rho \ll \rho$  is the density jump at the pycnocline.

If the initial wave is long enough, dispersive effects are negligible, and the propagation corresponds to a simple wave, every point of which propagates with the local velocity  $c(z)$ . From that, the parameters of the point in which the wave ‘breaks’ (i.e. its profile becomes vertical) can be found. For our purposes, it is sufficient to estimate the greater distance,  $x^*$ , from the shelf break as that at which the top of the tidal internal wave,  $z = z_{\max} = A$ , will overcome its frontal point where  $z = 0$ . It is easy to see that

$$x^* = \frac{c_0 L}{c(A) - c_0} = \frac{c_0 T}{3(\sqrt{1 + A/h} - 1)} \quad (2)$$

where  $L = c_0 T$  is the length of the wave front upon reflection from the shelf break and  $T$  is the duration of this front, of order few hours. Supposing that the

unperturbed upper-layer thickness  $h$  along the internal wave path from the shelf break to the observation point lies in the interval between 5 and 20 m (as can be concluded from figure 6), and the wave amplitude is  $A=1$  m (a reasonable value), we obtain  $x^*/L=3.5\text{--}14$ . To estimate  $c_0=\sqrt{g'h}$ , one needs to know the density jump at the pycnocline. Even taking  $c_0=0.5\text{ m s}^{-1}$  and  $h=20$  m, both of which are rather large values for coastal zones, for  $T=3$  h (one-fourth of the diurnal period), we obtain  $x^*=75$  km. This is considerably smaller than the distance between the observation site and the shelf break, and any realistic tidally generated internal wave breaks before approaching the observation point. After breaking, oscillations appear at the front due to dispersive effects, leading to the formation of a solitary wave group. From this we conclude that there is ample time for the observed wave group to have formed from a tidally generated internal wave propagating from the shelf break.

Next, we estimate the parameters of solitary waves in the observation site. We suppose that the scattering level coincides with the pycnocline. For nonlinear waves in a layer overlying deep water, the BO equation is often used (Ostrovsky and Stepanyants 1989). It has a known solution in the form of an 'algebraic' soliton:

$$z = \frac{A_s}{1 + (x - Vt)^2 / \Delta^2} \quad (3)$$

Here,  $A_s$  is the soliton amplitude,  $V$  is its propagation velocity, and  $2\Delta$  is the effective half-width (at the level of  $A_s/2$ ). The latter are related to  $A_s$  by

$$V = c_0(1 + 3A_s/8h) \quad \Delta = 4h^2/3A_s \quad (4)$$

From figure 3, one can take  $h=4$  m for the first impulse; then the impulses appear on the pedestal descending up to about 7 m, and the amplitudes of the next few impulses are between 3 and 5 m. This puts  $V$  in the range of  $1.3 c_0$  to  $1.5 c_0$  and  $\Delta$  in the range of 4.5–19 m, so the total width is in the range of 9–38 m. The full width of the observed pulses at half the amplitude is 20–25 m. It should be noted, however, that figure 3 presents a cross-section of the soliton train along the flight trajectory. It could be expected that actually the wave arrives at the observation point from the closest part of the shelf break line; indeed, the primary, barotropic tidal wave refracts at decreasing depths so that it tends to propagate normally to the shelf contour. From the area bathymetry (figure 2), we see that the closest part of the shelf contour lies at an angle  $\theta$  of  $30\text{--}60^\circ$  to the left of the flight track. Thus, the real soliton width is smaller than the observed one by the factor of  $\cos\theta$ . If we assume a representative angle of  $45^\circ$ , the theory predicts a range of 13–54 m for the observed width. The observed widths lie within this span. However, the observed ratios  $A/h$  may not be small enough to ensure the applicability of formula (3), which was derived assuming a small nonlinearity.

Models of strong, steady, solitary waves in deep water (Ostrovsky and Grue 2003) predict that their width has a weak dependence on amplitude in the range of interest, which is consistent with the data in figure 3. However, these theories predict larger soliton widths than observed and also larger than predicted by the Benjamin—Ono theory. This suggests that the observed wave is still at a transient stage where the formation of quasi-stationary solitary waves is not complete. At any rate, figure 3 indicates the existence of a strongly nonlinear, dispersive group of unipolar impulses.

From this single observation (as from most *in situ* data taken at a fixed point) it is not possible to infer the propagation speed of the wave. Without this information, we cannot determine the strength of the pycnocline. If the wave were closer to the point of generation, the travel time from the tidal cycle could be estimated. This wave had been propagating for several days, however, and it is not possible to determine in which tidal cycle it was generated. A second pass over the wave after a period of several hours could be used to get an estimate of the strength of the pycnocline from airborne lidar. If we had seen two such wave groups separated by a tidal period, we could have estimated the speed from the spatial separation. However, we did not see another wave group like this on this flight. This is not unusual in tidal solitary wave observations; indeed, the tide strength varies from one tidal cycle to another, and often only a strong, spring tide will generate significant internal waves. In other words, the conditions leading to the formation of this type of nonlinear internal wave group are not always present.

## 5. Conclusions

The main conclusion is that it is possible to observe nonlinear internal waves in the open ocean using an airborne lidar. A plankton layer associated with a pycnocline moving up and down with the vertical motion of the wave provides the lidar signal. The likely mechanism for the generation of the soliton is the nonlinear, offshore propagation of a strong internal wave generated by the interaction of the tide with the continental shelf. The observation was made at a sufficient distance from the shelf for this process for a single internal wave to have broken into a group of solitary impulses. The width of the waves is consistent with this interpretation, although it appears that they had not fully developed into quasistationary solitary waves. It was not possible to infer the strength of the pycnocline from this single observation, which makes the above mechanism of soliton group formation still hypothetical, albeit the most natural hypothesis. It would require a second observation to measure the speed of internal wave propagation.

## Acknowledgments

This work was supported by the NOAA NMFS Steller Sea Lion Research Initiative and the Exxon Valdez Trustee Council. The SeaWiFS image was provided by the SeaWiFS Project, NASA/Goddard Space Flight Center and ORBIMAGE. The SAR image was provided by William Pichel and Karen Friedman of the Alaska SAR Demonstration, NOAA NESDIS. The GAK13 data were provided by Seth Danielson of the University of Alaska, Fairbanks. The mission described was flown by Matthew Sebree of Dynamic Aviation.

## References

- ANSI, 1993, *Safe Use of Lasers, Standard Z-136.1* (New York: American National Standards Institute), p. 120.
- APEL, J.R., HOLBROOK, J.R., TSAI, J. and LIU, A.K., 1985, The Sulu Sea internal soliton experiment. *Journal of Physical Oceanography*, **15**, pp. 1625–1651.
- CHOI, W. and CAMASSA, R., 1999, Fully nonlinear internal waves in a two-fluid system. *Journal of Fluid Mechanics*, **396**, pp. 1–36.
- CHURNSIDE, J.H., WILSON, J.J. and TATARSKII, V.V., 1997, Lidar profiles of fish schools. *Applied Optics*, **36**, pp. 6011–6020.
- CHURNSIDE, J.H., WILSON, J.J. and TATARSKII, V.V., 2001, Airborne lidar for fisheries applications. *Optical Engineering*, **40**, pp. 406–414.

- COWLES, T.J., DESIDERIO, R.A. and CARR, M.-E., 1998, Small-scale plankton structure: persistence and trophic consequences. *Oceanography*, **11**, pp. 4–9.
- DUDA, T.F. and FARMER, D.M. (Eds), 1999, The 1998 WHOI/IOS/ONR internal solitary wave workshop: contributed papers. Technical Report, WHOI 99-07, Woods Hole Oceanographic Institute, Woods Hole, Massachusetts.
- GARRETT, C. and MUNK, W., 1979, Internal waves in the ocean. *Annual Reviews in Fluid Mechanics*, **11**, pp. 339–369.
- GRIMSHAW, R., 2002, Internal solitary waves. In *Environmental Stratified Flows*, R. Grimshaw (Ed.) (Boston, MA: Kluwer), pp. 1–27.
- HANSON, A.K. and DONAGHAY, P.L., 1998, Micro- to fine-scale chemical gradients and layers in stratified coastal waters. *Oceanography*, **11**, pp. 10–17.
- HOGUE, F.E., WRIGHT, C.W., KRABILL, W.B., BUNTZEN, R.R., GILBERT, G.D., SWIFT, R.N., YUNGEL, J.K. and BERRY, R.E., 1988, Airborne lidar detection of subsurface oceanic scattering layers. *Applied Optics*, **27**, pp. 3969–3977.
- KONYAEV, K.V. and SABININ, K.D., 1992, *Waves Inside the Ocean*. Saint Petersburg: Gidrometeoizdat] [in Russian].
- KREKOV, G.M., KREKOVA, M.M. and SHAMANAIEV, V.S., 1998a, Laser sensing of a subsurface oceanic layer. I. Effect of the atmosphere and wind-driven sea waves. *Applied Optics*, **37**, pp. 1589–1595.
- KREKOV, G.M., KREKOVA, M.M. and SHAMANAIEV, V.S., 1998b, Laser sensing of a subsurface oceanic layer. II. Polarization characteristics of signals. *Applied Optics*, **37**, pp. 1596–1601.
- LIU, A.K., HOLBROOK, J.R. and APEL, J.R., 1985, Nonlinear internal wave evolution in the Sulu Sea. *Journal of Physical Oceanography*, **15**, pp. 1613–1624.
- OSTROVSKY, L.A. and GRUE, J., 2003, Evolution equations for strongly nonlinear internal waves. *Physics of Fluids*, **15**, pp. 2934–2948.
- OSTROVSKY, L.A. and STEPANYANTS, YU A., 1989, Do internal solitons exist in the ocean? *Reviews in Geophysics*, **27**, pp. 293–310.
- PINGREE, R.D. and MARDELL, C.T., 1985, Solitary internal waves in the Celtic Sea. *Progress in Oceanography*, **14**, pp. 431–441.
- STANTON, T.P. and OSTROVSKY, L.A., 1998, Observations of highly nonlinear internal solitons over the continental shelf. *Geophysical Research Letters*, **25**, pp. 2695–2698.
- TREVORROW, M.V., 1998, Observations of internal solitary waves near the Oregon coast with an inverted echo sounder. *Journal of Geophysical Research*, **103**, pp. 7671–7680.
- VASILKOV, A.P., GOLDIN, Y.A., GUREEV, B.A., HOGUE, F.E., SWIFT, R.N. and WRIGHT, C.W., 2001, Airborne polarized lidar detection of scattering layers in the ocean. *Applied Optics*, **40**, pp. 4353–4364.
- WARREN, J.D., DEMER, D.A., MCGEHEE, D.E., DI MENTO, R. and BORSANI, J.F., in press, Biological and physical factors affecting the distribution of *Meganyctiphanes norvegica* and other zooplankton in the Ligurian Sea in late summer 2000. *Journal of Plankton Research*.
- WALKER, R.E., FRASER, A.B., MASTRACCI, L. and HOCHHEIMER, B.F., 1982, Optical sounding for internal waves on the ocean thermocline. *Oceans 82 Conference Record*, 20–22 September 1982 (Washington, DC: American Geophysical Union), pp. 247–250.
- ZHENG, Q., KLEMAS, V., YAN, X.-H. and PAN, J., 2001, Nonlinear evolution of ocean internal solitons propagating along an inhomogeneous thermocline. *Journal of Geophysical Research*, **106**, pp. 14083–14094.
- ZORN, H.M., CHURNSIDE, J.H. and OLIVER, C.W., 2000, Laser safety thresholds for cetaceans and pinnipeds. *Marine Mammal Science*, **16**, pp. 186–200.